Clin Orthop Relat Res (2009) 467:1678–1687
DOI 10.1007/s11999-009-0828-4

SYMPOSIUM: PAPERS PRESENTED AT THE 2008 MEETING OF THE MUSCULOSKELETAL INFECTION SOCIETY

Topographic Features Retained after Antibiotic Modification of Ti Alloy Surfaces

Retention of Topography with Attachment of Antibiotics

Constantinos Ketonis BS, Javad Parvizi MD, Christopher S. Adams PhD, Irving M. Shapiro DDS, PhD, Noreen J. Hickok PhD

Published online: 14 April 2009

Abstract Periprosthetic infection is increasingly prevalent in orthopaedics with infection rates of 2% to 15% after total hip arthroplasty. To effectively decrease bacterial attachment, colonization, and subsequent development of periprosthetic infection, we previously described a method to covalently bond vancomycin to smooth Ti alloy surfaces. To attach vancomycin, the Ti surface is first passivated to create a fresh oxide layer. Previously, passivation has been achieved with an H_2SO_4/H_2O_2 etch that can destroy the topography of the underlying implant. Passivation by hydrothermal aging as well as by H_2SO_4/H_2O_2 incubation produced a robust oxide layer, but only hydrothermal aging left the geometry unaltered. These hydrothermally passivated Kirschner wires and smooth or beaded Ti surfaces were chemically coupled with vancomycin. Antibiotic-coupled samples representing all three geometries were uniformly covered with antibiotic, resisted colonization by Staphylococcus aureus for longer than 8 hours, and retained their biocompatibility as assessed by normal attachment and morphology of preosteocytic MLO-A5 cells. Using this technique, we believe it is possible to passivate many complex implant designs/geometries as a first step toward covalent bonding of antibiotics or other bioactive factors.

One or more of the authors (JP, NJH) owns shares in SmartTech that could benefit from this technology; SmartTech did not fund any of this work. One or more of the authors have received grants from the National Institutes of Health (grants DE-13319 [IMS, CSA], DE-10875 [IMS, CSA], and AR-051303 [CSA, NJH, JP, IMS]), and the Department of Defense (grant DAMD17-03-1-0713 [CSA, NJH, JP, IMS]) for this study. Results presented are not the statement or policy of the funding agencies.

C. Ketonis, C. S. Adams, I. M. Shapiro, N. J. Hickok (✉)
Department of Orthopedic Surgery, Thomas Jefferson University, 1015 Walnut Street, Suite 501, Philadelphia, PA 19107, USA
e-mail: Noreen.Hickok@jefferson.edu

J. Parvizi
Rothman Institute of Orthopaedics, Thomas Jefferson University, Philadelphia, PA, USA

I. M. Shapiro, N. J. Hickok
Department of Biochemistry and Molecular Biology, Thomas Jefferson University, Philadelphia, PA, USA

Introduction

Over the last 50 years, metals and metal alloys have enjoyed great success in orthopaedics and dentistry [15, 32]. Their usefulness lies in their desirable physical and mechanical properties, including durability, low modulus of elasticity, excellent fatigue and tensile strength, and, most importantly, biocompatibility [7]. These metallic implants have evolved from simple supportive structures to bioactive surfaces that can actively modulate the host response. Specifically, the physical characteristics of the implant surface, namely its geometry and microtopography, influence the degree of osteointegration and cell response [8, 9, 19]. Optimizing these surfaces has resulted in enhanced bone fixation so the use of polymethylmethacrylate cements in total joint arthroplasties has become largely unnecessary [18].

Despite the success in manipulating the surface to predictably optimize the bone-biomaterial interface, little progress has been made in protecting these implants from periprosthetic infections (PPIs), which are increasingly prevalent after orthopaedic procedures and a cause of high patient morbidity [1, 27]. Importantly, PPI is believed to begin when biofilm-forming bacteria adhere to the implant

and proliferate to establish a biofilm colony [11]. These adherent bacteria are not only able to evade immune surveillance, but systemic antibiotics tend to be ineffective in eradicating the infection. This is probably the result of the inability of antibiotics to penetrate the secreted thick, polysaccharide-containing biofilm glycocalyx, but also because of the altered metabolic state of biofilm-entrenched bacteria [10].

To address this issue, we previously covalently bonded antibiotics to model metal surfaces to prevent bacterial adhesion [2–4, 12]. Antibiotic bonding requires, as a first step, production of a surface oxide layer, which we have achieved through passivation with H_2SO_4/H_2O_2; this method is corrosive and is thus poorly suited for preserving the complex geometries associated with implant design. After passivation, subsequent steps required to chemically couple antibiotics to the surface are noncorrosive and thus neither alter nor are dependent on geometric features.

We therefore asked (1) if passivation by hydrothermal treatment [18, 20, 21, 23, 24, 30] would produce equivalent etching to that of H_2SO_4/H_2O_2 treatment as assessed by scanning electron microscopy (SEM); (2) if both methods produced similar oxide layers as determined by contact angle measurements; (3) if the hydrothermally passivated surface supported chemical coupling of vancomycin (VAN) as assessed by immunofluorescence; (4) if this VAN attachment by chemical coupling was sufficiently robust to resist bacterial colonization; and (5) if these hydrothermally aged, VAN-coupled surfaces allowed for the attachment of osteoblastic cells as assessed by actin cytoskeletal integrity.

Materials and Methods

Ti alloy wires or Ti alloy disks that were half smooth and half beaded (sintered cpTi beads) were cleaned and an oxide layer formed by passivation either by incubation in H_2SO_4/H_2O_2 or by hydrothermal aging (Fig. 1). Methods of passivation were compared using SEM to assess obvious areas of etching or pitting. We next assessed oxide layer creation as surface hydrophobicity/hydrophilicity by measuring the static contact angle of water. We then used

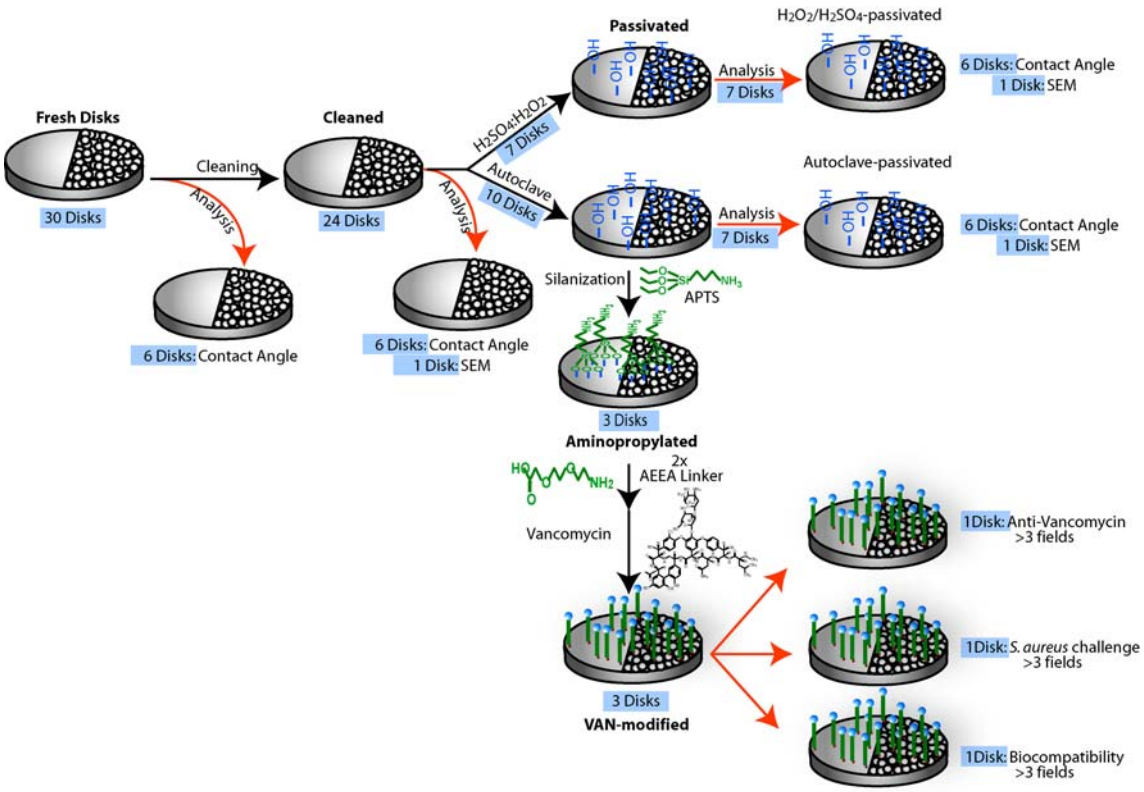

Fig. 1 The experimental design detailing the reaction scheme is shown. The entire reaction scheme was repeated in a total of three independent experiments. Approximately 30 disks are used in each experimental cycle. The disks are cleaned and seven are sampled for characterization. The remainder undergoes passivation either by acid etching or autoclave and seven from each group are sampled for further characterization. The remaining ten hydrothermally aged disks are used as a substrate for covalent addition of aminopropyltriethoxysilane (APTS), with seven removed for characterization. The remaining three disks are coupled with AEEA linkers, and vancomycin (VAN). Of the three synthesized disks, one of each is used for visualization of VAN distribution (anti-VAN) for challenge with S. aureus and for biocompatibility assessment. SEM = scanning electron microscopy.

hydrothermally aged surfaces to determine if this surface was suitable for covalent bonding of VAN and if it was able to retard bacterial colonization. Aminopropyltriethoxysilane (APTS) was bonded to the surface followed by sequential covalent addition of two linkers and VAN to the amino end of the APTS. The presence of surface-bound VAN as a function of surface geometry was detected using a specific antibody to VAN and visualized by immunofluorescence. We next challenged the hydrothermally aged, VAN-coupled surface (VAN-hTi) with Staphylococcus aureus (ATCC 25923) and the presence of viable, surface-adhered bacteria detected by fluorescent staining followed by digital imaging. Finally, VAN-hTi was evaluated for biocompatibility by examining cellular morphology and actin cytoskeletal architecture of MLO-A5 preosteocytic cells. Statistically, differences were assessed using contact angles that had been measured on six different disks from three independent passivation procedures. Visual assessments by SEM or immunofluorescence were performed on at least three distinct fields using disks from three different experiments. All experiments were repeated at least three times from samples taken from independent syntheses.

Metal surfaces were prepared for passivation by first cutting titanium alloy (Ti6Al4 V) wire (1-mm diameter wire; Goodman, Inc, Alexandria, IN) into 25-mm lengths (usually approximately 100 wires per synthesis); Ti smooth/beaded disks (33-mm diameter, usually approximately 10 per synthesis; Smith & Nephew, Memphis, TN) were used as supplied. Before passivation, all samples were cleaned by incubation in approximately 15% Alconox (Alconox Inc, New York, NY) in a shaking water bath for 1 hour. All samples were then washed with DI H_2O 10 times, washed four times with 1 M NaOH with sonication for 10 minutes each, and finally incubated twice with HCl:MeOH (50:50 v:v) with intermittent sonication (5 minutes sonication, 5 minutes shaking repeated throughout 30 minutes) followed by two brief rinses with DI H_2O. The cleaned surfaces were then passivated either (1) by adding concentrated H_2SO_4 dropwise to H_2O_2 to form a 50:50 mixture that was incubated with the Ti surfaces for 4 hours; temperature was kept to 10°C or less by incubation on ice; or (2) by autoclaving (121°C, 15 psi) for 30 minutes for a total of three times.

Attachment of VAN to the passivated Ti surfaces was performed according to published procedures [4] (Fig. 1). Briefly, passivated surfaces were reacted under argon with 5 mM APTS in anhydrous toluene (50°C, 16 hours, with mixing). Fmoc-[2-(2-aminoethoxy)-ethoxy]-acetic acid (Fmoc-AEEA) in dimethylformamide (DMF) was coupled to the APTS-Ti surface in the presence of O-(7-azabenzotriazole-1-yl)-1,1,3,3-tetramethyluronium hexafluorophosphate (HATU) and the Fmoc protecting group removed by treatment with 20% piperidine in DMF. A second Fmoc-AEEA linker was coupled to the AEEA-APTS-Ti surface as described, and finally VAN was added to the deprotected AEEA-AEEA-APTS-Ti surface in the presence of HATU (VAN-AEEA-AEEA-APTS-Ti = VAN-hTi) [4]. To ensure there was no trapping of reagents or air pockets in the beaded portion of the disks, samples were sonicated after each reaction and wash.

To visualize surfaces after passivation, samples were extensively rinsed with DI H_2O to remove salts and dried in a dessicator overnight. The smooth and beaded sides of the disks were visualized using SEM (1000× magnification; Hitachi TM-1000 SEM, Ibaraki, Japan). Images were assessed for surface pitting and overall surface topography before and after treatment. Visualizations were performed in at least three areas on each disk and two disks were assessed.

To measure static contact angle, a 10-μL drop of water was deposited onto smooth or beaded surfaces at different stages in their preparation. Drop appearance was then digitally recorded perpendicular to the surface and images analyzed using the angle measurement tool of Adobe® Photoshop® (Version 10; Adobe Systems Inc, San Jose, CA). Images and measurements were recorded for six different disks representing three independent syntheses.

VAN distribution on the different surfaces was determined by immunofluorescence. Specifically, disks and rods were incubated in phosphate-buffered saline (PBS) overnight to elute any nonattached, adsorbed antibiotic. They were then incubated in 10% fetal bovine serum (FBS) in PBS for 30 minutes to block nonspecific antibody binding followed by incubation with mouse anti-VAN IgG antibody (1:1000; US Biological, Marblehead, MA) in PBS for 16 hours at 4°C with slow rocking. Samples were rinsed three times with PBS followed by incubation in PBS for 15 minutes. Bound antibody was then detected by incubation with AlexaFluor 488-coupled donkey anti-mouse IgG (1:300; Molecular Probes, Invitrogen, Carlsbad, CA) in PBS for 1 hour at 25°C and washed three times with PBS followed by incubation in PBS for 30 minutes. Disks were digitally imaged by epifluorescence (Nikon Optiphot-2 with ImagePro software); rods were imaged using confocal laser scanning microscopy (Olympus Fluoview 300; Olympus America Inc, Center Valley, PA).

Bacterial adherence to the surfaces was determined by incubation with S. aureus (ATCC 25923). S. aureus were cultured in trypticase soy broth (TSB; BD Biosciences, San Jose, CA), shaken at 250 rpm at 37°C for 12 to 16 hours (overnight culture), and by comparison to a 0.5 McFarland standard (a turbidity standard corresponding to approximately 10^8 colony-forming units [cfu] of S. aureus), serially diluted to a final concentration of 1×10^4 cfu/mL. In parallel, after sterilization with 70% EtOH for 15 minutes, control and VAN-hTi surfaces were washed three times with TSB. Metal samples were incubated in 1 mL of

S. aureus (approximately 10^4 cfu) in TSB for 4 hours at 37°C without shaking. The medium was removed, planktonic and loosely adherent bacteria removed by washing with TSB three times, and surfaces reincubated for another 4 hours in fresh TSB to allow for proliferation of adherent S. aureus. Surfaces were then washed six times with PBS to remove nonadherent bacteria followed by staining with the Live/Dead BacLight™ Viability Kit (1:300 Molecular Probes; viable bacteria fluoresce green) for 30 minutes at room temperature. All samples were visualized by confocal laser microscopy.

Biocompatibility of the VAN-hTi surfaces was assessed by culturing of MLO-A5 preosteocytic cells. Control and VAN-hTi samples were sterilized by incubation in 70% EtOH for 15 minutes, washed three times with sterile PBS, treated with Modified Eagle's Medium (α-MEM), and then exposed to ultraviolet light for 10 minutes. In parallel, MLO-A5 cells were cultured on collagen-coated dishes until approximately 90% confluent. Cells were trypsinized, resuspended in α-MEM with 5% FBS and 5% BCS at 1×10^5/mL, and a 300-μL drop containing 30,000 cells deposited onto the sterilized, control, or VAN-hTi surfaces. Cells were allowed to attach for 2 hours after which additional media was added to the wells; cells were incubated in complete media for 2 days at 37°C, 5% CO_2. At 48 hours, cells were rinsed twice with PBS, fixed for 10 minutes with 4% paraformaldehyde, rinsed twice with PBS, incubated with 0.5% Triton-X for 10 minutes, and blocked in 1% FBS for 1 hour. The actin cytoskeleton was visualized by incubation in 5 U/mL of Alexafluor 488 conjugated phalloidin (Molecular Probes) in PBS for 30 minutes in the dark at room temperature; nuclei were counterstained with propidium iodide (1:300; Molecular Probes) for another 30 minutes. Samples were then rinsed and visualized using confocal laser microscopy.

Assessments of etching were performed visually using SEM. We determined differences in static contact angles between discs that were fresh, cleaned, or passivated by H_2SO_4:H_2O_2 or by hydrothermal aging using one-way analysis of variance and, more specifically, the pairwise multiple comparison procedure (Tukey test); normality test was passed with a $p > 0.2$. Assessments of bacterial attachment and osteoblastic cell attachment were qualitative and performed by comparison of multiple fields within many samples with representative micrographs shown in the figures; it is not the intention of these micrographs to establish magnitudes of differences.

Results

By SEM, the microtopography of the hydrothermally aged Ti appeared superior to that of H_2SO_4:H_2O_2-treated discs. Specifically, only machining marks were apparent on either the control smooth (Fig. 2A) or control beaded (Fig. 2B) surfaces. The overall arrangement and scoring of the machining appeared largely unchanged after autoclaving of either the smooth (Fig. 2C) or beaded surfaces (Fig. 2D). After treatment with H_2SO_4:H_2O_2, etching was apparent on smooth surfaces where the parallel machining lines were interrupted by areas of etching (Fig. 2E); the beaded surfaces showed surface pitting as well as some larger scale etching (Fig. 2F). SEM images of VAN-derivatized surfaces were similar to those of the parent passivated surface, suggesting that the chemistry used for VAN coupling did not further alter the surface (data not shown).

Both methods of passivation produced hydrophilic surfaces as assessed by measurement of contact angles (Fig. 3A). The fresh, control surfaces were the most hydrophobic with a 10-μL drop of dH_2O forming a contact angle of 70.5° ± 3.0° (Fig. 3B, Fresh); the drop did not spread, even on the beaded side of the surface, suggesting the surface was highly hydrophobic. After cleaning with Alconox, the surface became more hydrophilic as evidenced by a smaller contact angle (55.0° ± 3.2°; Fig. 3B, Cleaned), which was similar ($p = 0.125$) to that measured on the fresh surfaces. After H_2SO_4/H_2O_2 passivation, the contact angle had decreased to 26.1° ± 7.8° (Fig. 3B, H_2SO_4/H_2O_2; $p = 0.002$ compared with cleaned). There was a color change in the underlying Ti alloy disks that was not observed with the other methods. Finally, the autoclaved disk showed clear spreading of the droplet and a contact angle (28.8° ± 2.9°) that was indistinguishable ($p = 0.979$) from that of the H_2SO_4/H_2O_2 passivated disk (Fig. 3B, Autoclave). Taken together, these data suggest both the H_2SO_4/H_2O_2 and hydrothermal aging methods produce surfaces with comparable hydrophilicity.

After coupling VAN [4] to a hydrothermally aged Ti surface (VAN-hTi), its distribution, using an anti-VAN antibody, appeared uniform over the surface (Fig. 4). For all control surfaces (Fig. 4A–C), VAN staining was undetectable. When VAN distribution was examined on the smooth (Fig. 4D), beaded (Fig. 4E), and wire (Fig. 4F) VAN-hTi surfaces, a uniform bright signal was visualized indicating abundant VAN coverage.

The smooth VAN-hTi surfaces inhibited bacterial colonization after incubation with S. aureus ($C_i = 1 \times 10^4$ cfu) for 8 hours; smooth control surfaces were abundantly colonized with areas of patchy staining indicating biofilm formation (Fig. 5A–B). Similarly, control beaded surfaces were readily colonized by S. aureus; VAN-hTi beaded surfaces showed little detectable colonization (Fig. 5C–D). As a result of the irregularity of the underlying surface, large areas of reflectance could also be detected in the beaded samples. Finally, in agreement with the VAN-hTi disks, VAN-hTi wires showed little

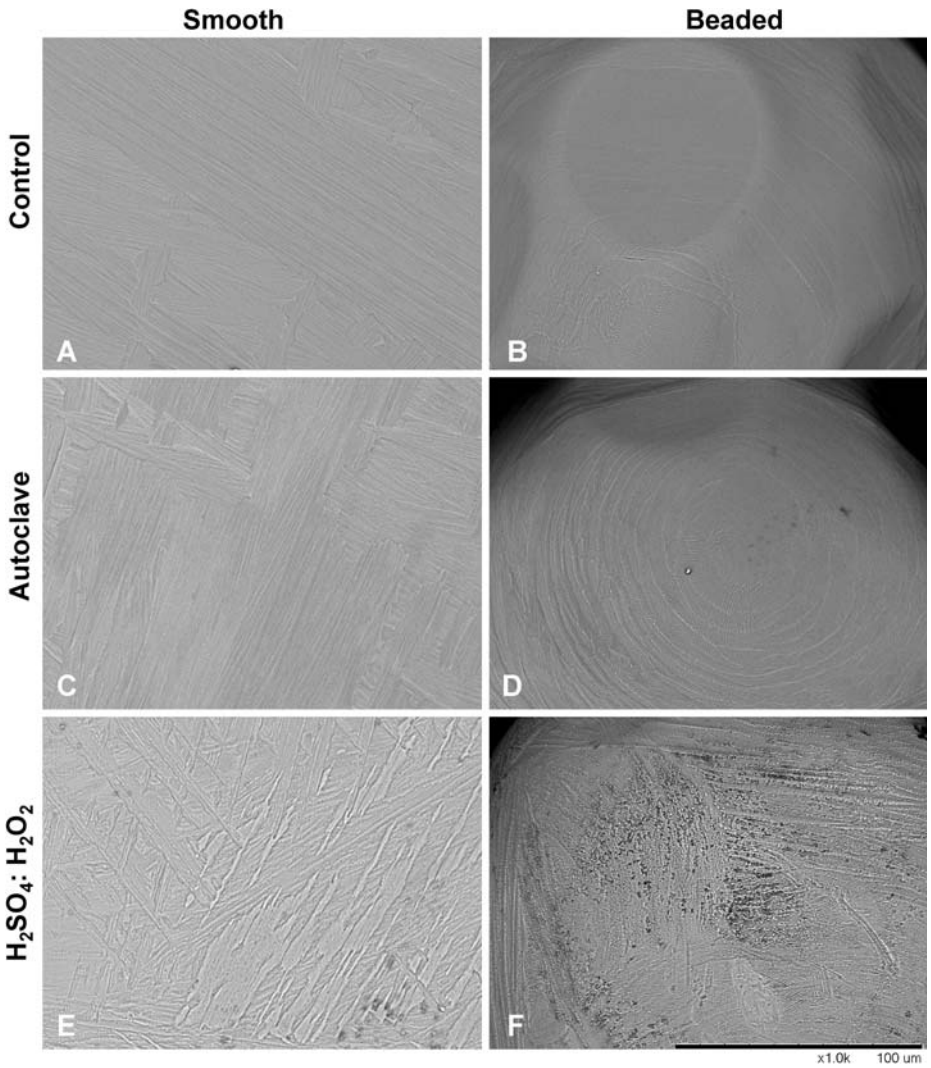

Fig. 2A–F Microtopographic assessment of smooth and beaded surfaces was performed by scanning electron microscopy imaging (1000×) and examined for changes in surface characteristics. (**A**) Control smooth surfaces showed parallel machining lines interrupted by small areas with crosswise lines. (**B**) Control beaded surfaces had flat surfaces with all surfaces showing shallow parallel grooves. (**C**) The hydrothermally passivated, autoclaved smooth disk also exhibited a fine array of lines with areas of interspersed crosswise lines. Appearances were within the range seen with control surfaces. (**D**) Beaded, hydrothermally passivated, autoclaved disks appeared similar to the control surfaces with concentric grooves apparent on the bead. (**E**) The surface of the H_2SO_4:H_2O_2-treated smooth disc showed obvious etching and deepening of the natural crevices of the metal. Dark areas indicating pitting can be seen at the bottom of the picture. (**F**) The etched, beaded surface exhibited extensive pitting (Magnification: 1000×, bar = 100 μm).

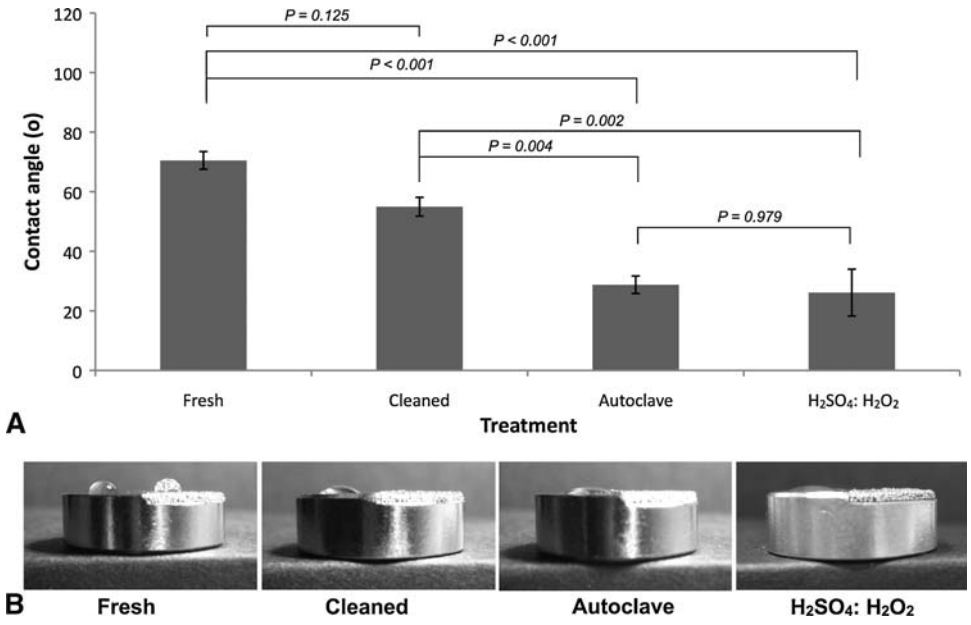

Fig. 3A–B Surface hydrophobicity was assessed as a function of treatment by placing a 10-μL water drop on disks that were untreated, cleaned, and passivated by H_2SO_4:H_2O_2 or passivated by autoclaving. (**A**) The contact angles are shown as measured from pictures of droplets on surfaces; statistical p values between groups are as noted. (**B**) Representative pictures of the droplets on the surfaces are shown. The decreasing contact angles obtained for the H_2SO_4:H_2O_2 and autoclaved conditions suggest these treatments are successful in creating a robust oxide layer.

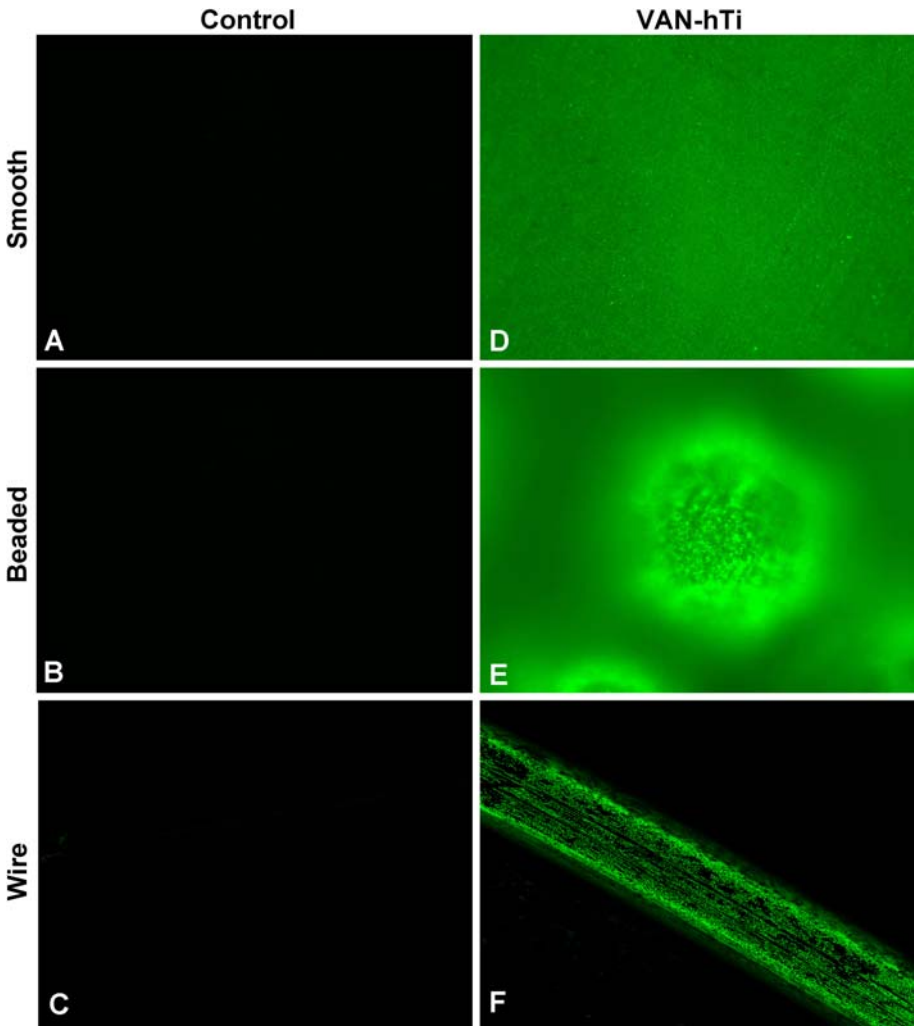

Fig. 4A–F Passivation by hydrothermal aging supports vancomycin (VAN) coupling that resists bacterial colonization. The oxide layer produced through autoclaving was used to couple linkers and VAN to the surface of smooth/beaded disks and Ti wires. No immunostaining could be detected on surfaces that had not been reacted with VAN. (**A**) Smooth control surfaces showed no VAN staining. (**B**) VAN staining was not apparent on control beaded surfaces. (**C**) Wire control surfaces also appeared free of signal. (**D**) Uniform VAN staining was apparent on the smooth VAN-hTi surfaces. (**E**) Abundant staining was apparent on the beaded surfaces with out-of-plane reflectance apparent. (**F**) Abundant staining was also visible on the VAN-hTi wires (Stain: primary antibody, mouse anti-VAN IgG; secondary antibody, AlexaFluor 488-coupled donkey anti-mouse IgG; original magnification: 20×).

colonization in sharp contrast to control wires that were abundantly colonized (Fig. 5E–F) and showed staining patterns suggestive of biofilm formation.

Finally, both control and VAN-hTi surfaces supported osteoblastic cell adhesion, suggesting equivalent biocompatibility. Smooth, control surfaces were colonized by MLO-A5 cells (Fig. 6A) with many cells retaining a rounded morphology and/or a cytoskeleton abundant in cortical actin staining; microspikes were apparent in multiple cells and probably indicated changing cell shape. MLO-A5 cells cultured on smooth VAN-hTi exhibited a range of sizes from small to large with abundant actin stress fibers. On the VAN-hTi surface, cells were well spread with fewer microspikes than control samples (Fig. 6B). On control beaded Ti surfaces, cells were well-spread with a trapezoidal shape (Fig. 6C) that was similar to that observed on VAN-hTi beaded samples (Fig. 6D); both control and Van-hTi samples showed similar distributions of cells. Overall, control and VAN-hTi surfaces were roughly equivalent in their ability to maintain normal cellular morphology.

Discussion

Titanium and titanium alloys are among the most widely used biomaterials in orthopaedic and dental implants [28]. Although these implants are highly engineered to optimize the bone-biomaterial interface [22], the topography of this interface is altered when coatings or modifications are applied. We have theorized that engineered surface features could be retained through the use of gentle passivation techniques, ie, hydrothermal aging. In this article, we have compared appearance and hydrophobicity of surfaces passivated using either a chemical method or hydrothermal aging. The hydrothermally aged surface was then further tested as a substrate for chemical coupling of the antibiotic VAN; success of the coupling and activity of this chemically coupled VAN was determined. Finally, we performed a limited evaluation of biocompatibility based on cell morphology and actin cytoskeletal architecture.

This study, although supportive of the use of hydrothermal etching, was limited both by the topography and by the nature of the bacterial colonization. First, the use of

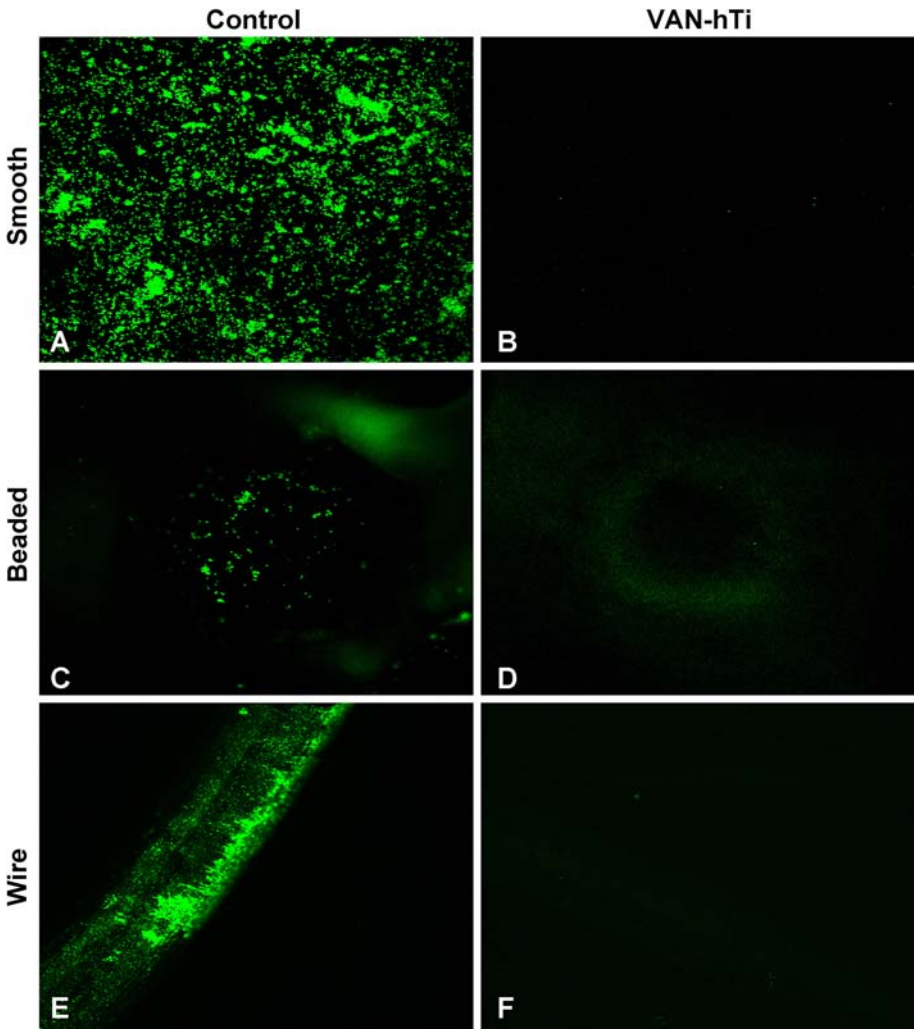

Fig. 5A–F VAN-hTi samples resist bacterial colonization. Control or VAN-hTi smooth or beaded surfaces or Kirschner wires were incubated with Staphylococcus aureus and rinsed and stained using the Live/Dead BacLight kit. (**A**) Control smooth surfaces were abundantly colonized with areas of intense staining that were characteristic of microcolony formation. (**B**) VAN-hTi smooth surfaces, which were imaged at the same settings as the control panels, showed no obvious bacterial colonization. (**C**) Beaded control surfaces showed areas of punctate staining that were visible at the top of the bead, which was the focal plane used for the confocal microscope. (**D**) VAN-hTi beaded samples show no punctate staining, although hazy green fluorescence is present as it is in the control samples and indicative of reflectance from the complex surface. (**E**) Kirschner wires were readily colonized as indicated by punctate green fluorescence that represents microcolony formations with the larger patchy stain suggestive of biofilm formation. (**F**) On VAN-hTi wires, no bacterial colonization can be visualized (Stain: Live/Dead BacLight Bacterial Detection kit; original magnification: 40×).

topographies that encompass curved surfaces with varying degrees of roughness, although allowing assessment of surface hydrophobicity through contact angle measurements, would not allow some of the more precise techniques for measurement of roughness such as atomic force microscopy. Nevertheless, the SEM images of the surfaces indicated clear etching, although the magnitude of the etching could not be determined. Second, the chemical coupling of VAN to the surface relied on immunofluorescent visualization of intensities and heterogeneities in surface coverage. Cleavage of the VAN from the surface would have allowed assessment of total amounts [3, 12], but the inaccuracy associated with comparing amounts on surfaces with markedly different surface areas and topographies would have rendered these measurements meaningless. Third, successful chemical coupling of VAN to the surface required that the VAN retain its activity against Gram-positive S. aureus, the predominant organism responsible for PPI. Measurement of adherent bacterial numbers can only be achieved through sonication and treatments with detergents that allow resuspension of the adherent bacteria [25]. These methods, however, are inherently inaccurate because only a subset of the bacteria is suspended by the sonication procedures (leaving the implant still colonized) and some bacteria remain in a biofilm metabolic state and fail to produce a colony on plating. Therefore, assessment with a viable dye, as we have done in this study, has been proposed as the only accurate method to assess surface colonization [14]. Fourth, the visual assessment for each of these determinations was based on sampling of three fields on a single disk/experiment (Fig. 1). However, the multiple observations on each disk are not independent. Finally, as noted in this article, toxicity assessments are limited to actin cytoskeletal architecture and cell shape. Additional markers of cell viability/toxicity as well as maturation markers would need to be assessed to thoroughly understand the effects of the different surfaces on biocompatibility.

As determined by SEM, hydrothermal passivation of Ti surfaces is less destructive than acid passivation on three test geometries: smooth, beaded, and a cylindrical pin. Retention of surface characteristics is essential for the

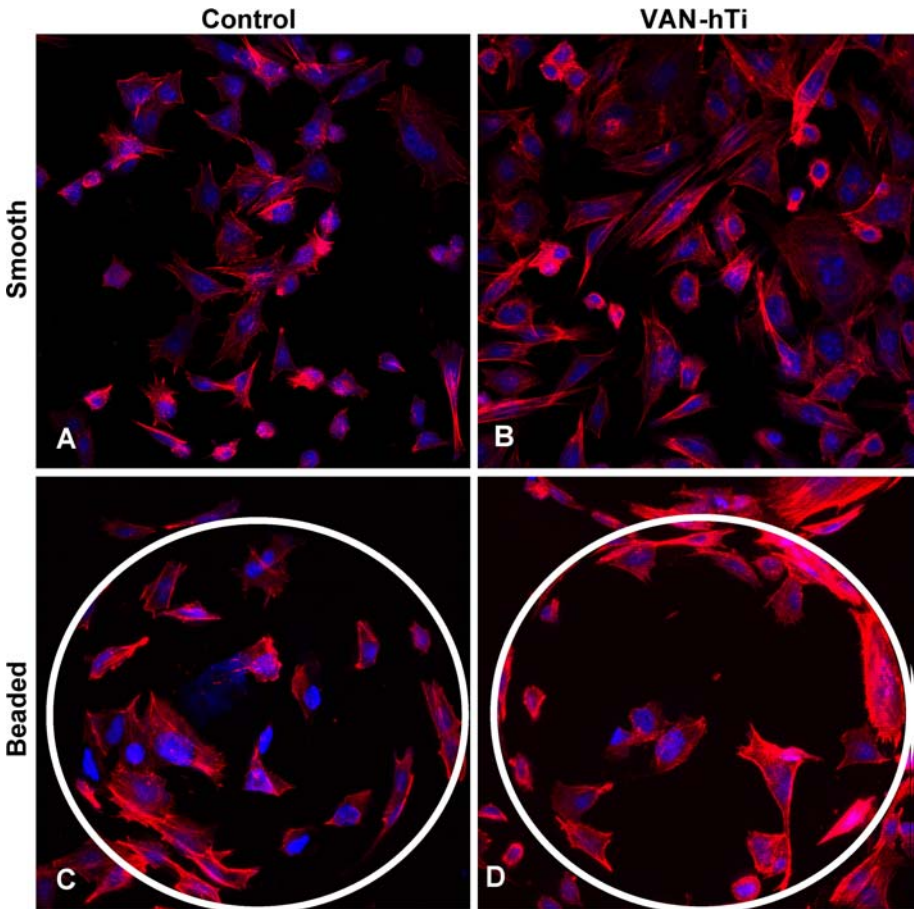

Fig. 6A–D VAN-hTi supports normal cellular morphology. Preosteocyte-like MLO-A5 cells were assessed for morphology and cytoskeletal architecture on the different surfaces. (**A**) MLO-A5 cells readily adhered to smooth, control surfaces with a number of cells exhibiting an array of actin stress fibers; other cells showed cellular extensions that are characteristic of cells undergoing shape or size changes. (**B**) MLO-A5 cells readily colonized the VAN-hTi surface with cell shapes ranging from small to more trapezoidal shapes. Actin stress fibers were apparent throughout as were cells bearing microspikes, presumably a sign of cell spreading. (**C**) Cells on control, beaded surfaces appeared well-spread with abundant actin staining. Some stress fibers were apparent as were short actin bundles. Morphology was within that normally observed for the MLO-A5 cells. (**D**) Cells seeded on beaded surfaces VAN-hTi surfaces showed abundant cellular colonization with a normal actin cytoskeletal network. Cell shape appeared normal (Stain: Actin cytoskeleton: Alexafluor 488 conjugated phalloidin, red; Nuclei: propidium iodide, blue; original magnification: 40×).

correct function of implants, many of which have a heterogeneous surface, whether resulting from engineered roughness/porosity, calcium phosphate coatings [6], collagen/hydroxyapatite coatings [31], BMP [16, 17] and RGD peptides [13] addition, or even drug-eluting polymer systems [26]. Hydrothermal aging retains the design features of the smooth, beaded, and cylindrical surfaces without additional pitting, suggesting it holds promise for application of technologies requiring covalent addition of bioactive agents to the implant surface. Thus, orthopaedic and dental implants that rely on a heterogeneous surface, usually comprised of smooth surfaces in which minimal friction is required, and rough surfaces in which good osseointegration and stability is the goal, can be used with this minimally destructive passivation technique.

SEM data suggested the hydrothermal aging was able to preserve the surface characteristics, whereas the contact angle measurements spoke to the equivalence of the oxide layers produced by both methods. These oxide layers are required for the chemical coupling steps in which the surface supports the formation of a self-assembled, cross-linked monolayer through reaction with APTS. This technique of measurement, however, could not address the thickness nor composition of the oxide layer, which will need to be determined in later experiments because such changes may be important for longevity of the surface modification.

Importantly, based on immunofluorescence, the oxide layer formed by hydrothermal aging is able to be successfully coupled with linkers and VAN. Because complex geometries, as represented by the beaded surface, are infiltrated with pores and microchannels, we found any synthesis using this type of surface requires additional sonication steps to ensure solvent and reactant access to these areas. VAN attachment was not characterized over the long term, and if hydrothermal aging becomes the method of choice for producing factor-bearing Ti surfaces, long-term stability studies will need to be performed. Nevertheless, the short-term assessments are in agreement with studies using the acid-etched surfaces that do indeed show long-term stability [4]. Importantly, to our knowledge, the reported lifespan, based on in vitro assessments, for the VAN-hTi far exceeds the finite lifespan of elution systems [4, 5, 29].

Sufficient VAN can be coupled to the hydrothermally passivated surface to render it resistant to bacterial colonization. In other studies, acid-etched surfaces are not only active in the presence of serum proteins [4], but against

bacterial numbers that exceed 10^7 cfu, numbers far higher than those experienced in an establishing infection. The bactericidal results of the VAN-hTi surfaces appear equivalent to those of the acid-etched surfaces and we expect equivalent activity in the presence of serum proteins. Given the prevalence of PPIs resulting from S. aureus activity, the activity of these surfaces against these high bacterial numbers promises a tool that can prevent establishment of infection over the long term and thus prevent the implant from becoming a source of continuing infection. The importance of this is illustrated in a previous study in which a H_2O_2:H_2SO_4-etched, VAN-modified Ti alloy showed no colonization in the presence of bathing concentrations of VAN; such a treatment models a successful antibiotic treatment of PPI [4]. In contrast, the untreated Ti alloy remained colonized by S. aureus, even in high concentrations of solution VAN, again modeling the refractoriness of established infections to antibiotic treatment. Thus, a long-term surface modification may not only keep the implant free from contaminating micro-organisms, but may be capable of maintaining an establishing infection in an antibiotic-sensitive state.

Finally, our biocompatibility assessments are based on morphology and the appearance of a cytoskeletal architecture consistent with the fibroblastic-like morphology of osteoblasts. Based on these promising studies, maturation experiments will need to be performed as will quantitative measurement of any toxicity. Importantly, cell morphology is a good predictor of toxicity and the experiments that we have described support the activity and biocompatibility of this VAN-hTi surface.

Taken together, the synthetic scheme we have outlined is applicable to smooth or roughened/beaded surfaces as well as wires. The elucidation of a means to chemically modify implants with retention of topography will allow the use of the existing implant designs to produce bioactive implants that retain their functional characteristics.

Acknowledgments We thank Smith & Nephew for manufacturing and supplying the smooth/beaded disks used in these studies.

References

1. Agerer F, Lux S, Michel A, Rohde M, Ohlsen K, Hauck CR. Cellular invasion by Staphylococcus aureus reveals a functional link between focal adhesion kinase and cortactin in integrin-mediated internalisation. *J Cell Sci.* 2005;118:2189–2200.
2. Antoci V, Adams CS, Hickok NJ, Shapiro IM, Parvizi J. Vancomycin bound to Ti rods reduces periprosthetic infection: preliminary study. *Clin Orthop Relat Res.* 2007;461:88–95.
3. Antoci V, Adams CS, Parvizi J, Ducheyne P, Shapiro IM, Hickok NJ. Covalently attached vancomycin provides a nanoscale antibacterial surface. *Clin Orthop Relat Res.* 2007;461:81–87.
4. Antoci V, King SB, Jose B, Parvizi J, Zeiger AR, Wickstrom E, Freeman TA, Composto RJ, Ducheyne P, Shapiro IM, Hickok NJ, Adams CS. Vancomycin covalently bonded to titanium alloy prevents bacterial colonization. *J Orthop Res.* 2007;25:858–866.
5. Arciola CR, Alvi FI, An YH, Campoccia D, Montanaro L. Implant infection and infection resistant materials: a mini review. *Int J Artif Organs.* 2005;28:1119–1125.
6. Bernstein A, Nöbel D, Mayr HO, Göbel F, Berger G, Ploska U, Gildenhaar R, Brandt J. Inhibition of mineralization by a calcium zirconium phosphate coating. *J Biomed Mater Res B Appl Biomater.* 2008;86B:422–429.
7. Bordji K, Jouzeau JY, Mainard D, Payan E, Netter P, Rie KT, Stucky T, Hage-Ali M. Cytocompatibility of Ti-6Al-4 V and Ti-5Al-2.5Fe alloys according to three surface treatments, using human fibroblasts and osteoblasts. *Biomaterials* 1996; 17:929–940.
8. Boyan BD, Batzer R, Kieswetter K, Liu Y, Cochran DL, Szmuckler-Moncler S, Dean DD, Schwartz Z. Titanium surface roughness alters responsiveness of MG63 osteoblast-like cells to 1 alpha, 25-(OH)2D3. *J Biomed Mater Res.* 1998;39:77–85.
9. Buser D, Schenk RK, Steinemann S, Fiorellini JP, Fox CH, Stich H. Influence of surface characteristics on bone integration of titanium implants. A histomorphometric study in miniature pigs. *J Biomed Mater Res.* 1991;25:889–902.
10. Costerton JW, Stewart PS, Greenberg EP. Bacterial biofilms: a common cause of persistent infections. *Science.* 1999;284: 1318–1322.
11. Darouiche RO. Treatment of infections associated with surgical implants. *N Engl J Med.* 2004;350:1422–1429.
12. Edupuganti OP, Antoci V Jr, King SB, Jose B, Adams CS, Parvizi J, Shapiro IM, Zeiger AR, Hickok NJ, Wickstrom E. Covalent bonding of vancomycin to Ti6Al4 V alloy pins provides long-term inhibition of Staphylococcus. *Bioorg Med Chem Lett.* 2007;17:2692–2696.
13. Ferris DM, Moodie GD, Dimond PM, Gioranni CW, Ehrlich MG, Valentini RF. RGD-coated titanium implants stimulate increased bone formation in vivo. *Biomaterials.* 1999;20:2323–2331.
14. Fux CA, Stoodley P, Hall-Stoodley L, Costerton JW. Bacterial biofilms: a diagnostic and therapeutic challenge. *Expert Rev Anti Infect Ther.* 2003;1:667–683.
15. Hanawa T, Sakamoto H, Tanaka Y. Biofunctional hybrid of titanium with polymers. *Mat Sci Forum.* 2007;539:563–566.
16. Jennissen H. Modification of metal surfaces and biocoating of implants with bone morphogenetic protein-2 (BMP-2). *Vopr Med Khim.* 1975;21:313–317.
17. Jennissen HP, Zumbrink T, Chatzinikolaidou M, Steppuln J. Biocoating of implants with mediator molecules: surface enhancement of metals by treatment with chromosulfuric acid. *Materwiss Werksttech.* 1999;30:838–845.
18. Kieswetter K, Schwartz Z, Dean DD, Boyan BD. The role of implant surface characteristics in the healing of bone. *Crit Rev Oral Biol Med.* 1996;7:329–345.
19. Kieswetter K, Schwartz Z, Hummert TW, Cochran DL, Simpson J, Dean DD, Boyan BD. Surface roughness modulates the local production of growth factors and cytokines by osteoblast-like MG-63 cells. *J Biomed Mater Res.* 1996;32:55–63.
20. Kilpadi DV, Lemons JE. Surface energy characterization of unalloyed titanium implants. *J Biomed Mater Res.* 1994;28: 1419–1425.
21. Kilpadi DV, Lemons JE, Liu J, Raikar GN, Weimer JJ, Vohra Y. Cleaning and heat-treatment effects on unalloyed titanium implant surfaces. *Int J Oral Maxillofac Implants.* 2000;15: 219–230.
22. Lincks J, Boyan BD, Blanchard CR, Lohmann CH, Liu Y, Cochran DL, Dean DD, Schwartz Z. Response of MG63 osteoblast-like cells to titanium and titanium alloy is dependent on surface roughness and composition. *Biomaterials.* 1998;19: 2219–2232.

23. Mante FK, Little K, Mante MO, Rawle C, Baran GR. Oxidation of titanium, RGD peptide attachment, and matrix mineralization in rat bone marrow stromal cells. *J Oral Implantol.* 2004;30: 343–349.
24. Pohler OE. Unalloyed titanium for implants in bone surgery. *Injury.* 2000;31(Suppl 4):7–13.
25. Trampuz A, Piper KE, Jacobson MJ, Hanssen AD, Unni KK, Osmon DR, Mandrekar JN, Cockerill FR, Steckelberg JM, Greenleaf JF, Patel R. Sonication of removed hip and knee prostheses for diagnosis of infection. *N Engl J Med.* 2007;357: 654–663.
26. Udipi K, Chen M, Cheng P, Jiang K, Judd D, Caceres A, Melder RJ, Wilcox JN. Development of a novel biocompatible polymer system for extended drug release in a next-generation drug-eluting stent. *J Biomed Mater Res A.* 2008;85:1064–1071.
27. Van de Belt H, Neut D, Schenk W, Van Horn JR, Van der Mei HC, Busscher HJ. Infection of orthopedic implants and the use of antibiotic-loaded bone cements. *Acta Orthop Scand.* 2001;72: 557–571.
28. Van Noort R. Titanium: the implant material of today. *J Mater Sci.* 1987;22:3801–3811.
29. von Eiff C, Kohnen W, Becker K, Jansen B. Modern strategies in the prevention of implant-associated infections. *Int J Artif Organs.* 2005;28:1146–1156.
30. Wang CC, Hsu YC, Su FC, Lu SC, Lee TM. Effects of passivation treatments on titanium alloy with nanometric scale roughness and induced changes in fibroblast initial adhesion evaluated by a cytodetacher. *J Biomed Mater Res A.* 2009;88:370–383.
31. Wang D, Chen C, He T, Lei T. Hydroxyapatite coating on Ti6Al4 V alloy by a sol-gel method. *J Mater Sci Mater Med.* 2008;19:2281–2286.
32. Williams DF. Titanium and titanium alloys. *Biocompatibility of Clinical Implant Materials.* Vol 1. Boca Raton, FL: CRC Press Inc; 1981:9–44.